AIAA SciTech Forum
6-10 January 2020, Orlando, FL
AIAA Scitech 2020 Forum

10.2514/6.2020-0859

Optimal Control Approach to Terrain Following Trajectory Generation

Shawn S. Stephens*, Joshuah A. Hess†, and Donald L. Kunz‡
Air Force Institute of Technology, Wright-Patterson Air Force Base, Ohio

This paper presents an optimal control formulation of the terrain following terrain avoidance path planning problem. The specific objective of this paper is to find the control which minimizes an aircraft's height above terrain as the aircraft flies from one side of a mountain range to the other. The flight path must avoid terrain and keep out zones constraints while satisfying the aircraft dynamic constraints. In this problem formulation USGS terrain elevation data was used to provide accurate and realistic terrain elevation data. A simplified aircraft model was developed using load factor rate and roll acceleration as control inputs eliminating the need to compute aerodynamic forces and moments. This formulation resulted in potentially flyable minimum height above terrain paths which were computed using the optimal control software GPOPS-II and non-linear problem solver IPOPT. The resulting paths were flown in a non-linear flight simulator to qualitatively assess flyability. The results of the flyability study showed the paths were flyable by aircraft with performance capabilities greater than or equal to the performance constraints used in the optimization routine.

Nomenclature

a_i	=	local latitude axis scale factor for KOZ_i	t_f	=	final time (sec)
a_c	=	centripetal acceleration $\left(\frac{ft}{sec^2}\right)$	U	=	body x-axis velocity $\left(\frac{ft}{sec}\right)$
a_s	=	speed of sounds $\left(\frac{ft}{s}\right)$	u	=	control inputs
b	=	wing span (ft)	V	=	body y-axis velocity $\left(\frac{ft}{sec}\right)$
b_i	=	local longitude axis scale factor for KOZ_i	V_∞	=	free stream airspeed $\left(\frac{ft}{sec}\right)$
c_i	=	local altitude axis scale factor for KOZ_i	W	=	body z-axis velocity $\left(\frac{ft}{sec}\right)$
h	=	altitude above mean sea level (ft)	$\mathbf{x}$	=	state vector
h_{AGL}	=	altitude above terrain (ft)	x_{si}	=	longitude coordinate of the center of KOZ_i
h_t	=	terrain altitude above mean sea level (ft)	y_{si}	=	latitude coordinate of the center of KOZ_i
g	=	gravitational acceleration $\left(\frac{ft}{sec^2}\right)$	z_{si}	=	altitude coordinate of the center of KOZ_i
KOZ_i	=	keep out zone identifier	ε_1	=	keep out zone vertical plane shape
N_{Z_x}	=	z-axis load factor component x	ε_2	=	keep out zone horizontal plane shape
P	=	body-axis roll rate $\left(\frac{rad}{sec}\right)$	ϕ	=	roll angle rad
p_E	=	position longitude component (ft)	θ	=	pitch angle rad
p_N	=	position latitude component (ft)	ψ	=	heading angle rad
q	=	state constraint weight			

I. Introduction

TERRAIN following and terrain avoidance have an important place in aviation. Military aviation emphasizes terrain following because aircraft near the ground are generally harder to observe and detect by an adversaries sensors.

*Captain, USAF, PhD Student, Department of Aeronautics and Astronautics
†Major, USAF, Assistant Professor, Department of Aeronautics and Astronautics
‡Professor, Department of Aeronautics and Astronautics

However, flying near the ground increases the overall risk to the aircraft because there is no room for mistakes and the consequence of a mistake is loss of the aircraft. Optimizing terrain following trajectories is difficult because the desired trajectory tends to activate a constraint, minimum height above terrain, for as much of the flight path as possible.

Terrain avoidance is often considered an analogue to terrain following because the same constraint, a minimum height above terrain, is key to the problem formulation. The objective of terrain avoidance is typically not to fly as close to the ground as possible. Rather, the objective in terrain avoidance is to navigate around terrain and arrive at a desired location, often a runway in a mountainous area. This paper focuses on terrain following as it typically presents the greater challenge with regard to incorporation of the terrain.

Optimal path planning often uses the path itself as the primary design variable by parameterizing the path coordinates [1]. However, performance constraints may be difficult to enforce because the performance characteristics of the aircraft must be transformed into geometric path constraints. In [2] this concern is alleviated by formulating the control inputs as the primary design variables. The careful selection of control inputs and limits may inherently output a flyable path and the use of geometric path constraints may not be required.

The primary difficulty of terrain following path planning is determining a method to evaluate height above terrain. A math model of these types of constraints is often developed in order to perform an optimization as opposed to using raw data which is often aggregated in a tabular database. In [3] a small aircraft maneuvers through an urban environment minimizing flight time while avoiding buildings. In [4] the landing path of an aircraft is optimized to minimize the jet engine noise perceived by the local population. In both of these cases the building and population density data were transformed into continuous math models. The downside to using math models to represent the data is that they are only a representation of reality and some, especially discontinuous datasets, are not suitable to representation by a model.

Discrete elevation data has been used in terrain following research since elevation data has been available [5]. Terrain following systems have also been fielded on operational fighter aircraft which utilize a radar to determine the terrain height in front of the aircraft [6]. In both of these cases, only the longitudinal axis is optimized/controlled and time to a desired waypoint is not considered. Today, tabular elevation data is available for most of the world but specifically for the entire continental United States at a resolution of $\frac{1}{3}$ arc-second which is approximately 10 meters depending on the Longitude via the United States Geologic Survey (USGS) National Elevation Dataset (NED) [7].

This paper formulates the terrain-following/terrain avoidance (TF/TA) path planning problem as an optimal control problem minimizing time and height above terrain, subject to aircraft dynamic, performance, altitude, and geographic keep out zone constraints. A simplified aircraft model is formulated using load factor rate and roll acceleration as control inputs eliminating the need for an aerodynamic model in the optimization routine. This simplified model is compared to a full six-degree of freedom simulation, JSBsim, to determine if the computed paths are potentially flyable [8]. Additionally, the terrain elevation is determined via a table lookup of the USGS NED during the optimization routine. Minimum altitude and minimum time problems are solved using the software package GPOPS-II and the nonlinear solver IPOPT [9, 10]. GPOPS-II is a general-purpose optimal control problem solver based in MATLAB. The software uses a variable-order adaptive Legendre-Gauss Radau quadrature collocation method to solve the transcribed nonlinear optimal control problem

The minimum time problem is formulated as a free final time problem while the minimum altitude problem is formulated as a fixed final time problem in order to analyze the solution's sensitivity to final time. The output of the minimum time problem is expected to resemble a terrain avoidance trajectory while the output of the minimum altitude problem is expected to resemble a terrain following trajectory. The state and control solution of the minimum time problem is then used as an initial guess for the minimum altitude problem. This provides a feasible initial guess for the minimum altitude problem. Finally, the resulting trajectories were flown by hand in the non-linear flight simulator FlightGear [11] using the JSBsim dynamics model to qualitatively assess the flyability of the trajectories.

Section II presents the formulation of the equations and constraints used in the optimization. Section III presents the mathematical problem statement. Section IV describes the approach taken to find a feasible solution. Finally Section V presents the optimization results.

II. Problem Formulation

The equations concerning aircraft motion are well known but the specific equations and assumptions used in this study are defined in this section. A top-down view of the problem scenario is presented in Fig. 1. The arrows represent the initial/final location and heading with the initial location in the bottom left of the map. The red circles represent the spherical keep out zones.

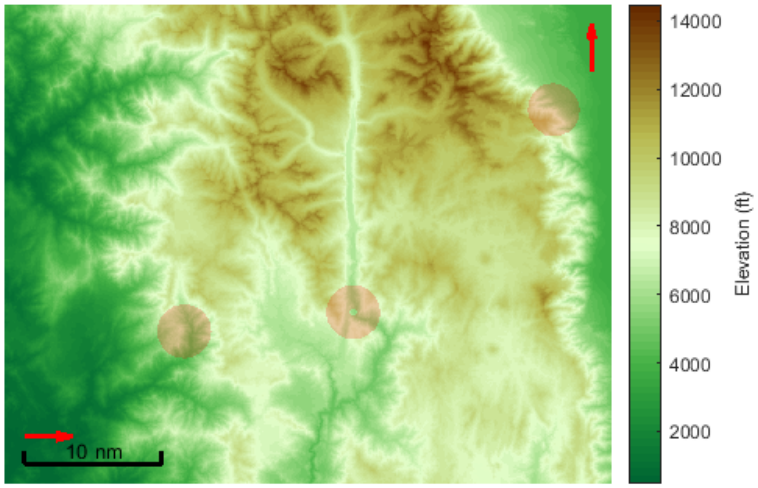

Fig. 1 Scenario Overview

A. Cost Function

The optimal control problem was divided into two separate problems with the same form of cost function. The first was a free final time, fixed final state minimum time problem. The second was a fixed final time, fixed final state minimum altitude problem. The cost function for this problem is given by Eq. (1) and was chosen to allow the problem to be easily converted from a minimum time to a minimum altitude problem by simply setting either q_{time} or q_{AGL} to zero. The height above terrain was chosen, as opposed to height above mean sea level, to include the nonlinear terrain calculation in the cost function itself.

$$J = \int_0^{t_f} q_{time} + q_{AGL} h_{AGL} \, dt \tag{1}$$

B. Control and Aircraft Assumptions

The aircraft is assumed to be a point mass traveling at a constant velocity. The control of the aircraft model is performed through roll acceleration and load factor rate. This assumption mimics the control of the aircraft while eliminating the direct computation of aerodynamics. Additionally, it is assumed there are no forces or moments which affect load factor or roll rate.

Roll acceleration was chosen because it is directly related to roll moment, representing realistic roll parameters. This model assumes a limit on the magnitude of roll acceleration and a limit on roll rate. Load factor rate was chosen because it allows for a continuous load factor state variable. The model assumes a limit on the magnitude of load factor rate in addition to limits on load factor itself.

C. State

The state of the aircraft is governed by the nonlinear aircraft equations of motion for p_N, p_E, and h given by Eq. (2) to Eq. (4) [12, p. 111]. The variables p_N and p_E are the North and East components of aircraft position in feet relative to the initial aircraft position. The variable h is geometric altitude in feet referenced to mean sea level. The equations are directly related to the terrain height lookup table and calculation of height above terrain.

$$\dot{p}_N = U\cos\theta\cos\psi + V(-\cos\phi\sin\psi + \sin\phi\sin\theta\cos\psi) + W(\sin\phi\sin\psi + \cos\phi\sin\theta\cos\psi) \tag{2}$$

$$\dot{p}_E = U\cos\theta\sin\psi + V(\cos\phi\sin\psi + \sin\phi\sin\theta\sin\psi) + W(-\sin\phi\cos\psi + \cos\phi\sin\theta\sin\psi) \tag{3}$$

$$\dot{h} = U\sin\theta - V\sin\phi\cos\theta - W\cos\phi\cos\theta \tag{4}$$

1. Simplification from Aircraft Equations of Motion

Equations (2) to (4) are simplified by assuming constant velocity and $\alpha = \beta = 0$. Thus $\theta = \gamma$ and $\psi = \chi$. The assumptions result in the x-component of velocity U equal to the freestream velocity of the aircraft, $U(t) = V_\infty$, and the other velocity components equal to zero; $V = W = 0$.

$$\dot{p}_N = V_\infty \cos\gamma \cos\chi \tag{5}$$

$$\dot{p}_E = V_\infty \cos\gamma \sin\chi \tag{6}$$

$$\dot{h} = V_\infty \sin\gamma \tag{7}$$

The roll and heading angle equations are developed from aircraft turn rate performance equations [13]. The equation for turn rate around an arbitrary axis is simply the centripetal acceleration in the specified axis divided by velocity. The general form of the equation is shown in Eq. (8).

$$\omega = \frac{a_c}{V_\infty} \tag{8}$$

The turn rate equations are typically used for steady state performance analysis by making assumptions on ϕ and θ [13]. ϕ, θ, and the normal acceleration are allowed to vary rather than assuming a constant altitude turn, a pull-up, or a pull-down. It is assumed that the stability axis pitch rate and yaw rate are only affected by N_Z generated by the aircraft and the force of gravity via Eq. (8). This assumption is shown in Eq. (9) and Eq. (10).

$$Q = \frac{g(N_Z - \cos\phi\cos\gamma)}{V_\infty} \tag{9}$$

$$R = \frac{g\cos\gamma\sin\phi}{V_\infty} \tag{10}$$

Finally, these stability axis rates are transformed to Euler Angle rates using the transformation matrix Eq. (11) and Eq. (12) [12].

$$C = \begin{bmatrix} 1 & \sin\phi\tan\gamma & \cos\phi\tan\gamma \\ 0 & \cos\phi & -\sin\phi \\ 0 & \frac{\sin\phi}{\cos\gamma} & \frac{\cos\phi}{\cos\gamma} \end{bmatrix} \tag{11}$$

$$\begin{bmatrix} \dot{\phi} \\ \dot{\gamma} \\ \dot{\chi} \end{bmatrix} = C \begin{bmatrix} P \\ Q \\ R \end{bmatrix} \tag{12}$$

The results of these calculations are

$$\dot{\phi} = \frac{PV_\infty\cos\gamma + gN_Z\sin\phi\sin\gamma}{V_\infty\cos\gamma} \tag{13}$$

$$\dot{\gamma} = \frac{g(N_Z\cos\phi - \cos\gamma)}{V_\infty} \tag{14}$$

$$\dot{\chi} = \frac{gN_Z\sin\phi}{V_\infty\cos\gamma}. \tag{15}$$

The dynamics of N_Z are assumed to be a single integrator with N_Z rate being a control. The dynamics of ϕ are assumed to be a double integrator with roll acceleration being a control. These dynamics are summarized by

$$\dot{N}_Z = u_{\dot{N}_Z} \tag{16}$$

$$\dot{\phi} = P \tag{17}$$

$$\dot{P} = u_{\dot{\phi}}. \tag{18}$$

The terrain elevation is calculated with a table lookup based on the current latitude and longitude of the aircraft. The aircraft height above terrain is then calculated by Eq. (19).

$$h_{AGL}(t) = h(t) - h_t(p_N, p_E) \tag{19}$$

D. Constraints

The terrain constraint of this problem is enforced using the height above terrain based on the table lookup of the elevation dataset. Additionally, simple side bounds were applied to the N_Z state and P state. The keep out zones are enforced using superquadrics as defined by Eq. (20). The formula used outputs with a value equal to one when the point (p_N, p_E, h) is on the surface of the keep out zone, less than one when inside the keep out zone, and greater than one when outside of the keep out zone [14].

$$1 - \left(\left(\frac{p_E(t) - x_{si}}{a_i} \right)^{\frac{2}{\varepsilon_2}} + \left(\frac{p_N(t) - y_{si}}{b_i} \right)^{\frac{2}{\varepsilon_2}} \right)^{\frac{\varepsilon_2}{\varepsilon_1}} + \left(\frac{h(t) - z_{si}}{c_i} \right)^{\frac{2}{\varepsilon_1}} \leq 0 \tag{20}$$

The keep out zone shape is defined by the parameters ε_1 and ε_2 where a value of 1 for either parameter creates an elliptical shape in the corresponding plane and a value of 0.1 creates a rectangular shape in the corresponding plane. However, initial iterations showed the solver had a difficult time solving the problem due to numerical problems when using a shape parameter of 0.1. Thus a parameter of 1 was used for all keep out zones making them ellipsoidal. The scaling factors a_i, b_i and c_i are used to control the size of the keep out zone while x_{s_i}, y_{s_i}, and z_{s_i} control the position of the keep out zone. The locations and sizes of the keep out zones were selected to ensure the minimal time path would activate at least one of the keep out zone constraints.

E. Boundary Conditions

The terrain data used in this problem encompass a portion of the Sierra Nevada mountains and were specifically selected because it includes low valleys on either side of a high mountain range. The initial and final location were selected to optimize the path over large terrain elevation differences. The attitude of the final condition was chosen to roughly simulate parameters which would be desired on an initial approach to a local airfield. The boundary conditions are summarized in Table 1. An overview of the problem setup is shown in Fig. 1 which includes the keep out zones and a top down representation of the initial and final states.

Table 1 Problem Boundary Conditions

Parameter	Initial	Final
Latitude	$36.1°$	$36.543° \pm 1000\ ft$
Longitude	$-118.9°$	$-118.046° \pm 1000\ ft$
Altitude	$1500\ ft$	$5200\ ft$
Roll Angle	$0\ rad$	$0 \pm 0.1\ rad$
Roll Rate	$0\ \frac{rad}{sec}$	$0 \pm 0.1\ \frac{rad}{sec}$
Load Factor	$1g$	$1 \pm 0.2g$
Pitch Attitude	$0\ rad$	$-0.0873 \pm 0.1\ rad$
Heading	$\frac{\pi}{2}\ rad$	$\pm 0.1\ rad$

III. Optimization Problem Statement

Minimize:

$$J = \int_0^{t_f} q_{time} + q_{AGL} h_{AGL}\ dt \tag{21}$$

Subject to the dynamic constraints:

$$\dot{p}_N = V_\infty \cos\gamma \cos\chi \tag{22}$$
$$\dot{p}_E = V_\infty \cos\gamma \sin\chi \tag{23}$$
$$\dot{h} = V_\infty \sin\gamma \tag{24}$$
$$\dot{\phi} = \frac{PV_\infty \cos\gamma + gN_Z \sin\phi \sin\gamma}{V_\infty \cos\gamma} \tag{25}$$
$$\dot{P} = u_{\dot{P}} \tag{26}$$
$$\dot{N}_Z = u_{\dot{N}_Z} \tag{27}$$
$$\dot{\gamma} = \frac{g(N_Z \cos\phi - \cos\gamma)}{V_\infty} \tag{28}$$
$$\dot{\chi} = \frac{gN_Z \sin\phi}{V_\infty \cos\gamma} \tag{29}$$

height above terrain constraint:

$$500 - h_t \leq 0 \tag{30}$$

state bounds:

$$0 \leq N_Z \leq 4 \tag{31}$$
$$-\pi \leq P \leq \pi \tag{32}$$
$$-\frac{\pi}{2} < \gamma < \frac{\pi}{2} \tag{33}$$

keep out zone constraints [14]

$$1 - \left(\left(\frac{p_E(t) - x_{si}}{a_i} \right)^{\frac{2}{e_2}} + \left(\frac{p_N(t) - y_{si}}{b_i} \right)^{\frac{2}{e_2}} \right)^{\frac{e_2}{e_1}} + \left(\frac{h(t) - z_{si}}{c_i} \right)^{\frac{2}{e_1}} \leq 0 \tag{34}$$

terminal constraint

$$\mathbf{x}(t_f) - \mathbf{x}_f = 0 \tag{35}$$

and control bounds

$$u_{\dot{N}_Z} \in [-3, 3] \tag{36}$$
$$u_{\dot{\phi}} \in \left[-\frac{\pi}{4}, \frac{\pi}{4} \right]. \tag{37}$$

Note: the specific bounds detailed in this formulation apply to Section V.B. Some values are changed during the sensitivity study as described in Section V.C.

IV. Solution Approach and Methodology

A. Path Optimization

The minimum time problem used an initial guess of a straight line from the initial point to the end point. This guess is clearly not feasible since it passes directly through the terrain however, GPOPS-II was able to converge to a locally optimal solution to the minimum time problem using this guess.

The minimum altitude problems were setup as a fixed final time to examine the change in minimum altitude trajectories as the fixed time was increased. The minimum altitude problem proved more difficult to solve since the objective was to put the trajectory on the terrain constraint for as much as the path as possible. The initial guess for each minimum altitude problem was the minimum time solution. The GPOPS-II settings for all solutions are given in Table 2.

Solution convergence tended to be highly dependent on the scaling method and derivative level. The derivative level was initially chosen as second to include the hessian and provide the solver with the most information. This setting was

successful in converging the minimum time solution. However, the setting was not successful for the minimum altitude problem. The large number of collocation points added due to the terrain constraint tended to cause solver crashes when computing the second derivative matrices, thus the $first$ derivative option was chosen for the minimum altitude problems. Additionally, the IPOPT and mesh iteration limit was increased from the default levels to allow the minimum altitude solution a better chance to converge.

Table 2 GPOPS-II Solver Settings

Mesh Method	hp-LiuRao	NLP Solver	IPOPT
Min. # of Collocation Points	3	NLP Solver Tolerance	1×10^{-6}
Max. # of Collocation Points	7	NLP Solver Iteration Limit	2000
Sigma	0.5	Derivative Level	second/first*
Mesh Iteration Limit	12	Derivative Dependencies	sparseNaN
Collocation Method	RPM-Integration	Scaling Method	automatic-hybridUpdate
*second for minimum time. first for minimum altitude			

B. Quantitative Comparison of Simplified Model to Full Nonlinear Model

The simplified equations of motion described by Eq. (5) to Eq. (7) and Eq. (13) to Eq. (15) are useful in that they are not functions of aircraft mass and aerodynamics. However, it is necessary to show they produce dynamics which are close enough to a model which includes aircraft aerodynamics to conclude that the path computed by the optimization is potentially flyable.

A high performance aircraft, F-16, was flown manually in the FlightGear flight simulator[11] using a JSBsim model [8]. A variety of maneuvers were flown to include terrain following. The output of this simulation was then fed into the simplified equations of motion and the applicable parameters were then compared. The first comparison was of the Euler angle rates. The nonlinear model rates were computed using Eq. (12) with the stability axis rate data from the nonlinear model. The simplified model rates were computed using Eq. (13) to Eq. (15) with all parameters coming from the nonlinear model. The second comparison calculated $\dot{N}_Z$ and P from the nonlinear simulation and used those parameters as the control input to the simplified model. The model was then integrated assuming the same initial conditions. The comparison results are presented in Section V.

C. Path Flyability Evaluation

The flyability of the computed paths was qualitatively evaluated using the FlightGear flight simulator [11]. The goal of the evaluation was to determine how well a human piloting a nonlinear aircraft model could follow the computed path's latitude, longitude, and altitude. The computed path control was not used during the evaluation.

The path was imported into FlightGear as 400 ft diameter rings with a sphere indicating the optimal path bank angle as shown in Fig. 2. The spherical bank angle indicator was used to provide upcoming turn information to the simulator pilot. The rings were spaced at 5 second intervals based on the planned speed of the aircraft. The evaluation was conducted by attempting to fly through the rings while adhering to the bank angle limit used in the path computation and maintaining airspeed near the planned airspeed.

The aircraft models used had similar performance characteristics at the flown speed as the aircraft type used to compute the path. The JSBsim C-130 and F-16 models were used to conduct this evaluation. The design of the JSBsim F-16 model allowed for the modification of the control law N_Z limits. These limits were modified to to correspond to the planned N_Z limits plus 0.5 G.

V. Results

A. Model Comparison

The comparison showed that the simplified model compared well to the nonlinear model (JSBsim) although the model error increased as the model assumption violations increased. The predominant model assumptions were constant

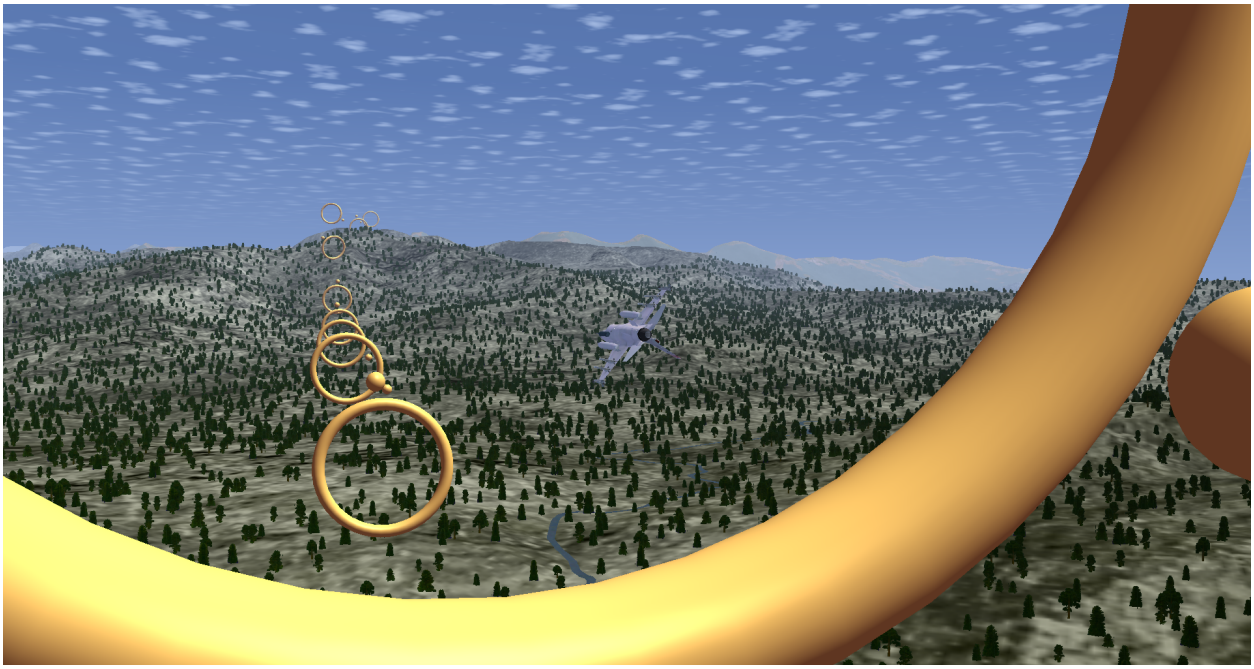

Fig. 2 FlightGear Study Screenshot

velocity, zero angle of attack, and zero angle of sideslip. The results of the angular rate comparison were calculated from the entire 9 minute simulation and are presented in Table 3.

Table 3 Model Error: Angular rates (Nonlinear-Simplified)

	Mean Error $\frac{rad}{s}$	Standard Deviation $\frac{rad}{s}$
$\dot{\phi}$	0	0.03
$\dot{\gamma}$	0	0.08
$\dot{\chi}$	0	0.08

The simplified model performed well under conditions similar to the assumptions made in their derivation. Four one-minute simulation segments were chosen for analysis and the results are presented in Table 4. The velocity range and angle of attack range are presented as a means to quantify how well the segment matched the model assumptions. The roll rate did not appear to affect the error although multiple full command rolls were performed in the simulation. The data shows that under approximately 10 degrees angle of attack and 200 $\frac{ft}{sec}$ of velocity change, the models matches well and it could be reasonably assumed that the nonlinear model could make up for the observed error and follow the simplified models path. The constraints imposed in this optimization problem adhere to these ranges, therefore it is deduced that paths computed in this optimization are potentially flyable.

Table 4 Model Error: Position and Altitude after 60 seconds (Simplified-Nonlinear)

Velocity Range $\frac{ft}{sec}$	α Range (deg)	Position Error (ft)	Altitude Error (ft)
585 to 757	-1.3 to 8.5	1661	-243
694 to 744	0.4 to 3.4	510	-143
410 to 864	0.9 to 21.1	2268	978
835 to 1097	0 to 16.1	2552	2370

B. Path Optimization

Figure 3 presents a top-down view of five GPOPS-II solutions. Four of the five solutions achieved the desired GPOPS-II mesh tolerance of 0.001 while the 530 second fixed time run only achieved a tolerance of 0.003. IPOPT was able to find an optimal solution for the minimum time problem however, only near-optimal feasible solutions were obtained for the minimum altitude problems. The solutions appear to follow the terrain well and it is likely the highly non-linearity of the terrain was a contributor to the convergence failure. All solutions adhered to the constraints.

Table 5 presents a summary of problem solutions. As expected, the average height above terrain decreases as the fixed final time is increased, however there is a limit to this decrease. This makes sense logically as there is likely a minimum achievable minimum height above terrain based on the roughness of the terrain. Lengthening the path from the minimum time solution causes the path to approach the terrain but at some point the path cannot get any lower due to the roughness of the terrain and simply lengthens to meet the fixed final time constraint. In this scenario it appears that solutions with fixed times greater than 530 seconds will likely have a mean height above terrain near 600 ft.

Table 5 Results Summary

	q_{time}	q_{AGL}	$t_f\,(sec)$	Mean $h_{AGL}(ft)$	Computation Time (min)
Min Time	1	0	502.16 (free)	2657	9
Min Alt	0	1	502.2 (fixed)	2630	46
Min Alt	0	1	515 (fixed)	634	72
Min Alt	0	1	530 (fixed)	602	88
Min Alt	0	1	545 (fixed)	608	69

In Fig. 3 we can see the minimum altitude solutions diverge from the minimum time solution as their fixed final time is increased. As the cost function only incorporates height above terrain, the paths appear to follow the "smoothest" terrain. The top down view of the minimum time path shows a relatively straight path with horizontal turns only used to navigate the keep out zones and achieve the boundary conditions.

The side view, as seen in Fig. 4, shows an expected altitude profile where the path changes as little as possible except to avoid the terrain and keep out zones. The turns in the altitude profile which are over 500 ft above the terrain of the minimum time path at approximately 150 seconds and 450 seconds are due to the keep out zones. A validation of the keep out zone constraint may be seen in Appendix Fig. A1 and a visualization of the aircraft trajectory around the keep out zone is presented in Appendix Fig. A2.

The control for the minimum time problem appears to follow Pontryagin's Minimum Principle as a bang-bang controller but is not displayed as it is very active [15]. Multiple 360-degree rolls were observed but did not coincide with pitch changing maneuvers (the aircraft rolled but decreased N_Z in such a way which caused ψ and θ to not change). Each 360-degree roll is likely creating a local minimum in the optimization. The realistic remedy would be to apply roll acceleration in the opposite direction. In the optimization routine this remedy would likely cause a small increase in cost or a terrain violation.

Although the behavior may not affect the cost of the optimization, decreasing N_Z during a roll is typically not performed in aircraft as it can cause engine issues due to a loss of oil pressure [16]. The practical remedy is to either limit N_Z during rolls or to limit the bank angle to prevent a roll. The later was studied in the sensitivity analysis section.

The estimate of the Hamiltonian is nearly constant indicating the minimum time solution is locally minimal. The Hamiltonian estimate is computed using the estimated costates output by GPOPS-II and the standard equation for the Hamiltonian [15].

A comparison of the minimum time solution to a minimum altitude solution was made with the time fixed to 502.2. While the minimum time solution was 502.16 seconds the minimum altitude failed to converge at that exact time but the small increase in fixed time allowed convergence. Figure 3 shows the latitude and longitude of the two paths are nearly identical and Fig. 4 shows the altitude component of the minimum altitude optimized path is also nearly identical to the minimum time path as expected. There is a slight downward shift in the path around 300 seconds due to the small change in time and the change in cost function. Finally, the computed path length is also identical supporting the validity of both solutions.

The altitude profile, load factor, and roll angle for the 530 second fixed time minimum altitude problem are presented in Fig. 5. The data for the 515 second fixed time problem is similar but the average height above terrain is slightly higher as presented in Table 5. The maximum height above terrain for the 530 second profile is 1831 ft and the maximum

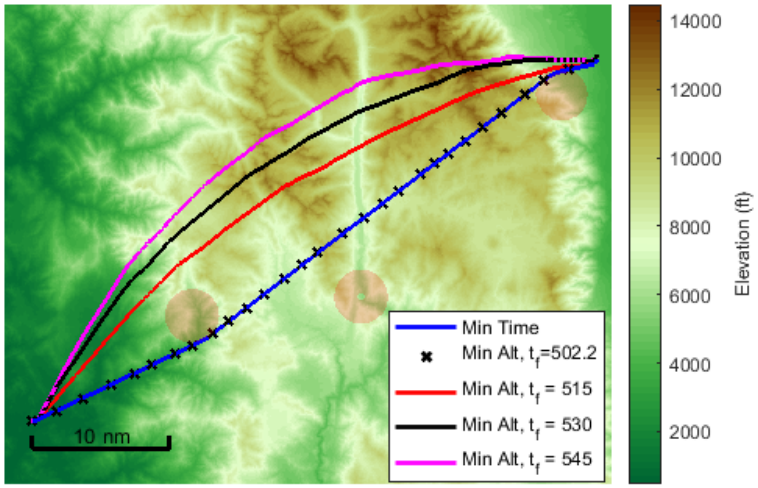

Fig. 3 Solution Trajectories

height above terrain for the 515 second profile is 2216 ft. Both maximums occur at the same valley which can be seen in Fig. 5 just before 350 seconds. In Fig. 3 we can see this valley near the middle of the map.

The raw control of the solutions are not presented because they behave as a bang-bang controller for nearly the entire time of flight. However, it is observed that the load factor itself does not behave the same way. The mean load factor for this solution is approximately 1.5g. The load factor quickly touches the limit a number of times during the trajectory however, the limit is sustained only twice during the flight; during the initial and final turn.

The roll angle is relatively active and often completes a full turn once any substantial roll rate is achieved. This behavior is similar to the rolls observed in the minimum time profile. However, the minimum altitude solution contained two distinct types of rolls. The first were similar to those observed in the minimum time optimization where ψ and θ did not change much during the roll. The second type of roll coincided with large θ and ψ changes and typically occurred near a peak in the terrain. This behavior matches the intuitive maneuver a pilot may make when crossing a ridge or mountain peak by rolling inverted and increasing N_Z to better follow the terrain.

The altitude profile follows the terrain very well except in the few cases of valleys which were too narrow to enter

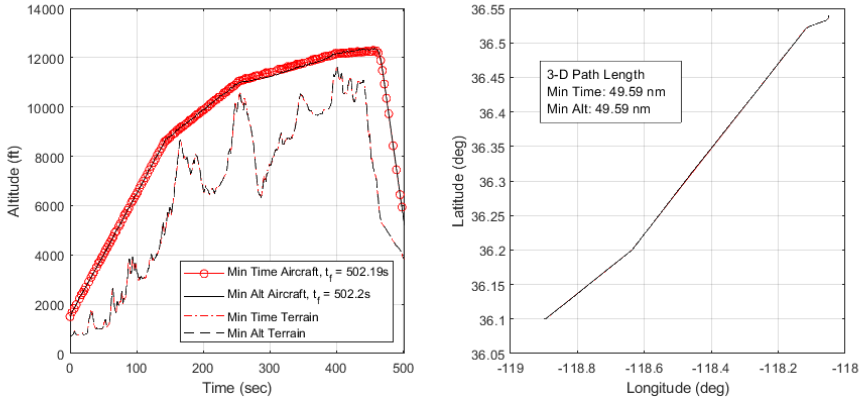

Fig. 4 Minimal Time and Minimal Altitude Solution Comparison

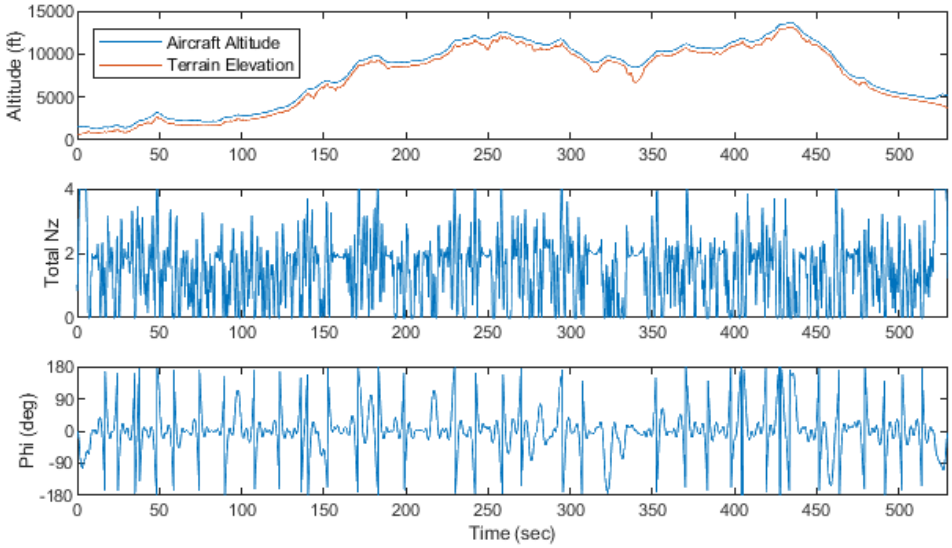

Fig. 5 Minimal Altitude, $t_f = 530s$, Summary

and exit without violating the altitude constraint. This is the desired behavior of a terrain following path. Finally, no aircraft performance constraint was violated indicating that the paths are potentially flyable by an aircraft with those performance capabilities ($\dot{N}_Z$, N_Z, $\dot{P}$, and P).

C. Sensitivity Analysis

The sensitivity analysis studied variations in velocity, aircraft limitations, and bank angle limits in order to determine if flyable paths could be computed for multiple types of aircraft. Three velocities were chosen which represented a low, medium, and high speed aircraft. The aircraft limitations used were maximum load factor, maximum load factor rate (pitch control), maximum roll rate (integral of roll control) and maximum roll acceleration. The aircraft limits used in the sensitivity analysis are presented in Table 6; the minimum load factor for each type was 0.2 G. The limits were chosen to represent a light cargo, jet trainer, and fighter jet type aircraft (for example a C-130J, T-6A, and F-16 respectively[17]). The fighter type aircraft was not analyzed at low speed as it is assumed the aircraft would not have the assumed type of performance at those low speeds.

Table 6 Aircraft Limits

Aircraft	Max N_Z	Max $\lvert\dot{N}_Z\rvert$ $(\frac{g}{sec})$	Max $\lvert P\rvert$ $(\frac{rad}{sec})$	Max $\lvert\dot{P}\rvert$ $\frac{rad}{sec^2}$
1	2.5	1	0.52	0.24
2	4	3	3.14	1.41
3	6	6	3.49	2.20

A bank angle limit comparison was also included due to multiple 360-degree rolls observed in the initial optimization solutions and the observed "roll and pull" behavior which appeared to improve the solution's ability to follow terrain.

The comparison was also made for the minimum time sensitivity study however the bank angle limit did not have an affect on the minimum time. This is because the extraneous rolls did not occur with large changes in θ or ψ and appeared to be extraneous artifacts of the optimization. Therefore the minimum time sensitivity results presented all have a bank angle limitation. A bank angle limit of 120 degrees was used for all runs as it is a common low level flight operational limit [18].

The settings and results for the minimum time sensitivity runs are presented in Table 7. Velocity has the largest impact on the minimum time, as expected, since constant velocity is assumed and the aircraft ends up traveling on nearly the same path. However, aircraft type has a small but observable impact on the minimum time. This result is primarily

due to the increased N_Z limit as can be seen by the maximum N_Z of the run always reaching the limit. This allows turns to be made more quickly and the time not flying straight is minimized. The roll rate limit was determined to have a lesser effect since 2 of the 3 aircraft were never limited by roll rate.

Table 7 Minimum Time Sensitivity Results

Settings			Results			
Speed ($\frac{ft}{sec}$)	Aircraft	ϕ Limit (rad)	t_f	Min N_Z	Max N_Z	Max P
340	1	2.09	884.6	0.4	2.5	0.52
340	2	2.09	883.7	0.2	4.0	1.54
600	1	2.09	503.3	0.5	2.5	0.52
600	2	2.09	501.9	0.4	4.0	1.48
600	3	2.09	501.3	0.2	6.0	1.97
800	1	2.09	378.8	0.2	2.5	0.52
800	2	2.09	377.4	0.2	4.0	1.64
800	3	2.09	376.7	0.4	6.0	1.92

The settings and results for the minimum altitude sensitivity runs are presented in Table 8. The fixed times for the minimum altitude runs were set to be approximately 6% greater than the minimum time. A simple statistical analysis of the minimum altitude sensitivity results showed that the aircraft type and bank angle limit were significant predictors of the observed mean height above terrain. They were both inversely proportional to the result. Additionally, aircraft velocity squared was also significant in predicting mean height above terrain although the predictor has a small coefficient indicating a small effect on the result.

Table 8 Minimum Altitude Sensitivity Results

Settings			Results				
$V(\frac{ft}{sec})$ / $t_f\,(sec)$	Acft.	$\phi_{Lim}\,(rad)$	Mean $h_{AGL}(ft)$	Max N_Z	Max $P(\frac{rad}{sec})$	Rolls > ϕ_{Lim}	Max $\dot{h}\ \frac{ft}{min}$
340 / 940	1	2.1	719.0	2.5	0.52	0	7137
340 / 940	1	125.7	702.9	2.5	0.52	0	7438
340 / 940	2	2.1	702.0	4.0	1.73	0	7434
340 / 940	2	125.7	612.7	4.0	3.14	37	10004
600 / 530	1	2.1	729.3	2.5	0.52	0	10878
600 / 530	1	125.7	677.5	2.5	0.52	0	15228
600 / 530	2	2.1	638.5	4.0	2.11	0	13908
600 / 530	2	125.7	589.6	4.0	3.14	53	16714
600 / 530	3	2.1	617.4	6.0	2.83	0	14677
600 / 530	3	125.7	581.3	6.0	3.49	64	18382
800 / 402	1	2.1	887.0	2.5	0.52	0	16001
800 / 402	1	125.7	787.2	2.5	0.52	3	16260
800 / 402	2	2.1	703.7	4.0	2.26	0	15199
800 / 402	2	125.7	619.6	4.0	3.13	40	25241
800 / 402	3	2.1	655.4	6.0	3.01	0	20266
800 / 402	3	125.7	573.6	6.0	3.49	56	27298

The relationship of an increase in aircraft performance to a decrease in average height above terrain is expected. Additionally, an increase in aircraft performance correlates with an increased number of inverted rolls when the bank angle is unlimited. This supports the previously observed behavior that terrain is better followed by rolling inverted and increasing load factor, "rolling" and "pulling", than by remaining upright and decreasing load factor (from 1 g).

The relationship of bank angle limit to mean h_{AGL} is expected as the aircraft can create a tighter turn by creating a positive pitch rate than with a negative pitch rate due to the asymmetric N_Z limits. In the roll limited case, this resulted in pushes to 0.2 G during 90 degree banks. This has the effect of a 1G turn, due to gravity, towards the ground while flying in a straight line due to the 0.2G push. The behavior is best shown in Fig. 6 as the limited aircraft tends to "push" to the minimum N_Z limit while banked during rapid decreases in terrain elevation while the unlimited bank run has the aircraft roll inverted and "pull" to the maximum N_Z. The unlimited aircraft is closer to the terrain during this section of the path which is more clearly seen at approximately 410 seconds.

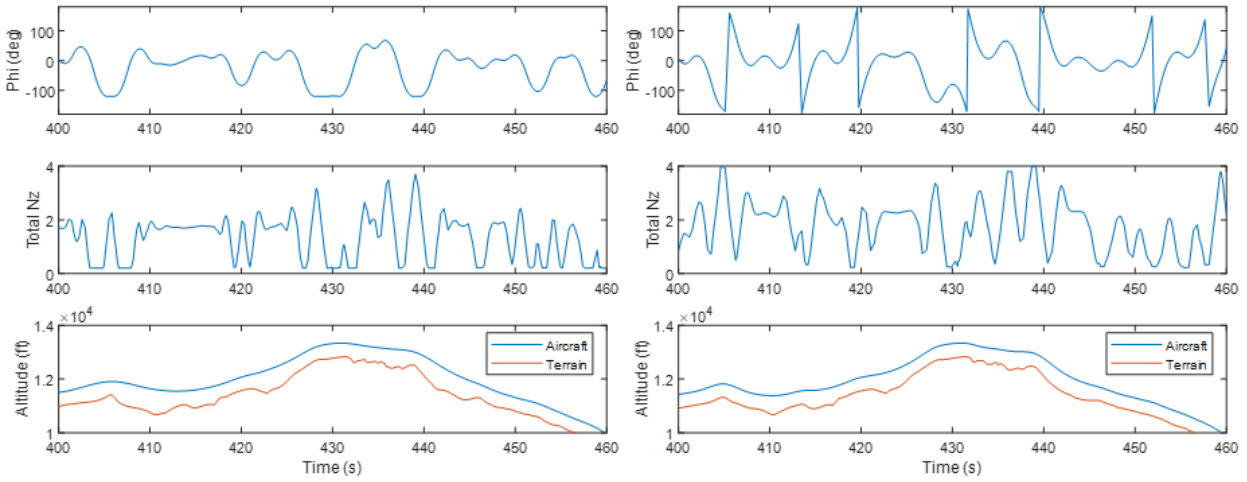

Fig. 6 Bank Limit (Left) v. No Bank Limit (Right)

The effect of aircraft speed on mean height above terrain is less intuitive. When aircraft performance is held constant, it is intuitive that the average height above terrain should increase with speed. This is because turn rate capability decreases with speed if load factor capability and the aircraft Euler Angles remains the same; Eq. (9). This capability can be mapped to turn radius when combined with aircraft speed. There is then a minimum turn radius the aircraft can follow. It appears that there is a limit where the capability of the aircraft is greater than the size of the major terrain features. However, small terrain features such as sharp increases and decreases whose size is on the order of 100 ft, will never be able to be followed by aircraft traveling at the speeds studied in this paper. Thus below a certain speed, any change in average height above terrain is likely due to the location of the path rather than the speed at which it was flown.

The minimum altitude runs typically had a maximum climb angle of 20-30 degrees although the limit imposed by the optimization was 90 degrees. The observed climb angle of 20-30 degrees corresponds to feasible climb rates for the type 2 and 3 aircraft but not the type 1 aircraft when looking at typical aircraft climb rate performance [17].

A secondary sensitivity analysis was run limiting the maximum climb angle to 5.7 degrees; the minimum climb angle was unchanged at -90 degrees. The new climb angle limit corresponds to a climb rate limit of 2026 $\frac{ft}{min}$, 3575 $\frac{ft}{min}$, and 4767 $\frac{ft}{min}$ for the low, medium, and high speed runs respectively. The results of this analysis was the mean height above terrain for every run was increased 80-524 ft with no other relationship observed.

D. Flyability Study

The flyability study qualitatively showed that the computed paths were able to be flown within a 200 ft radius using aircraft which had the same or greater performance than the limits used to compute the path. In general, the bank unlimited paths appeared to have less error than the limited paths. The bank limited paths included a significant number of "roll and push" maneuvers which are not typical aircraft maneuvers. The bank angle information, in the form of a sphere as shown in Fig. 2, was necessary to fly any of the paths as an indicator of future turn direction.

The higher speed paths were easier to fly than the lower speed path which is likely due to the simplified model assumptions. Specifically, the model assumes zero angle of attack and the simulator angle of attack is lower at higher speeds better representing the model assumptions. The slow speed pitch unlimited and limited paths were flown by the C-130 model. The pitch unlimited model was unable to be flown at the desired speed, as expected, due to performance limitations. The pitch limited path was easily flown and was representative of a terrain avoidance flight path.

VI. Conclusion

This paper presented an optimal control TF/TA path planning problem formulation utilizing interpolated terrain elevation. Minimum time and minimum altitude trajectories were computed across a mountain range subject to aircraft performance, height above terrain, and keep out zone constraints. Locally optimal and near optimal trajectories were obtained but required significant computation time.

A quantitative analysis of the assumptions which simplified the equations of motion in this paper was made to determine how well they compare to a 6 degree of freedom nonlinear aircraft model. The simplified model compared well with the nonlinear model and it was concluded that trajectories produced by the simplified model were potentially flyable by an aircraft with the same or greater performance characteristics.

A sensitivity analysis was performed using realistic aircraft aerodynamic and performance constraints which showed trajectories may be computed over a wide range of aircraft aerodynamic and performance limitations. These paths were then qualitatively evaluated in a flight simulator. The computed trajectories are all potentially flyable by aircraft with aerodynamic and climb performance capabilities which adhere to the assumed performance bounds used in the optimization. Additionally, the climb rate limited paths showed the ability to generate flyable terrain avoidance paths for aircraft with limited climb performance.

Further work in this area would be to investigate the costates of the optimization to determine if a near optimal online terrain follower may be developed from this problem formulation. Additionally, the inclusion of velocity control, performance, and fuel use data may allow the formulation of a combination minimum altitude and minimum fuel problem.

References

[1] Tsourdos, A., White, B., and Shanmugavel, M., *Cooperative Path Planning of Unmanned Aerial Vehicles*, John Wiley & Sons, Ltd, 2011.

[2] Kamyar, R., and Taheri, E., "Aircraft Optimal Terrain/Threat-Based Trajectory Planning and Control," *Journal of Guidance, Control, and Dynamics*, Vol. 37, No. 2, 2014, pp. 466–483. doi:10.2514/1.61339, URL https://doi.org/10.2514/1.61339.

[3] Zollars, M. D., Cobb, R. G., and Grymin, D. J., "Optimal Path Planning for SUAS Target Observation through Constrained Urban Environments using Simplex Methods," *Proceedings of the American Control Conference*, Vol. 2018-June, 2018, pp. 5094–5099. doi:10.23919/ACC.2018.8430987.

[4] Udani, J. P., Mall, K., Grant, M. J., and Sun, D., "Optimal Flight Trajectory to Minimize Noise During Landing," *55th AIAA Aerospace Sciences Meeting*, 2017, pp. 1–14. doi:10.2514/6.2017-1180.

[5] Funk, J. E., "Optimal-path precision terrain-following system," *Journal of Aircraft*, Vol. 14, No. 2, 1977, pp. 128–134. doi:10.2514/3.58755.

[6] SITZ, T., "F-15E terrain following test results," *Orbital Debris Conference: Technical Issues andFuture Directions*, American Institute of Aeronautics and Astronautics, Reston, Virigina, 1990. doi:10.2514/6.1990-1299, URL http://arc.aiaa.org/doi/10.2514/6.1990-1299.

[7] United States Geological Survey, "The National Map Viewer," , 2017. URL https://viewer.nationalmap.gov.

[8] Berndt, J., "JSBSim: An Open Source Flight Dynamics Model in C++," *AIAA Modeling and Simulation Technologies Conference and Exhibit*, American Institute of Aeronautics and Astronautics, Reston, Virigina, 2004. doi:10.2514/6.2004-4923, URL http://arc.aiaa.org/doi/10.2514/6.2004-4923.

[9] Patterson, M. A., and Rao, A. V., "GPOPS-II," *ACM Transactions on Mathematical Software*, Vol. 41, No. 1, 2014, pp. 1–37. doi:10.1145/2558904, URL http://dl.acm.org/citation.cfm?doid=2684421.2558904.

[10] A.Wachter, and L.T.Biegler, "On the Implementation of a Primal-Dual Interior Point Filter Line Search Algorithm for Large-Scale Nonlinear Programming," *Mathematical Programming*, Vol. 106, No. 1, 2006, pp. 25–57.

[11] FlightGear Project, "FlightGear Flight Simulator," , 2019. URL https://flightgear.org.

[12] Stevens, B. L., Lewis, F. L., and Johnson, E. N., *Aircraft control and simulation: Dynamics, controls design, and autonomous systems: Third edition*, Wiley-Blackwell, 2015. doi:10.1002/9781119174882.

[13] Bossert, D. E., Morris, S. L., Hallgren, W. F., and Yechout, T. R., *Introduction to Aircraft Flight Mechanics*, American Institute of Aeronautics and Astronautics, 2012. doi:10.2514/4.862069.

[14] Jaklič, A., Leonardis, A., and Solina, F., *Segmentation and Recovery of Superquadrics*, Vol. 20, Springer Netherlands, 2000. doi:10.1007/978-94-015-9456-1, URL http://link.springer.com/10.1007/978-94-015-9456-1.

[15] Kirk, D., *Optimal Control Theory*, Dover Publications, Inc., Mineola, New York, 1998.

[16] EXTRA Flugzeugproduktions- und Vertriebs- GmbH, "EXTRA 300 Pilot Operating Handbook," Tech. rep., 2006. URL https://www.extraaircraft.com/docs/service/POHEA300CUS2006-09-20.pdf.

[17] *Jane's All the World's Aircraft: Development and Production 2018-2019*, Jane's Information Group, 2018.

[18] United States Air Force, "AFI-11-2F-16V3," , 2017. URL https://static.e-publishing.af.mil/production/1/af{_}a3/publication/afi11-2f-16v3/afi11-2f-16v3.pdf.

Appendix

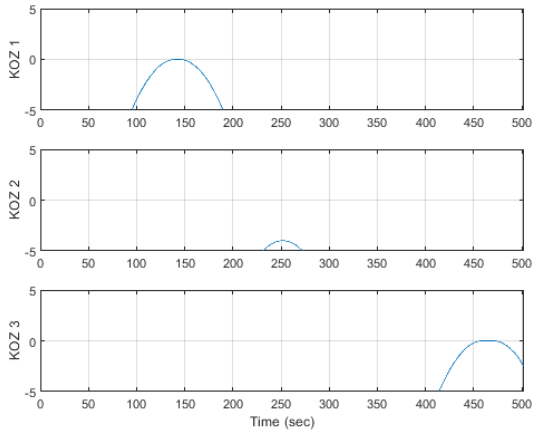

Fig. A1 Minimal Time Trajectory Keep Out Zone Parameter

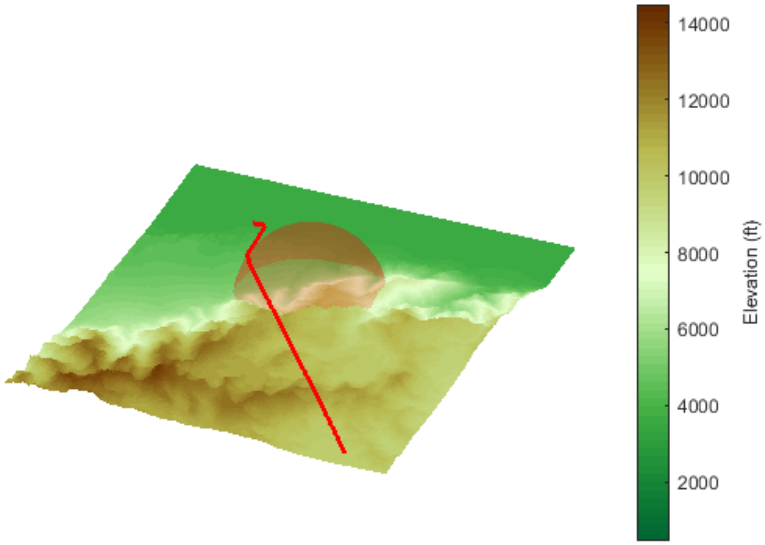

Fig. A2 Minimal Time Trajectory Keep Out Zone 3D view (KOZ 3)